Sedimentation of vesicles: from pear-like shapes to microtether extrusion

Z-H. Huang[1, 2, 3], M Abkarian[4] and A Viallat[1,2, 3] *

[1] INSERM U600, 163, Avenue de Luminy, case 937, 13288 Marseille, cedex09, France

[2] CNRS UMR6212, Marseille, France

[3] Université de la Méditerranée, Marseille, France

[4] Laboratoire des Colloïdes Verres et Nanomatériaux UMR 5587, CNRS/UM2, CC2 34095 Montpellier Cedex 5, France

E mail: annie.viallat@inserm.fr

PACS: 87.16.D- 47.15.G-

Submitted to New Journal of Physics

Abstract : We study the sedimentation of buoyant giant lipid vesicles in a quiescent fluid at velocities ranging from 5 to 20 μm/s. Floppy vesicles are deformed by the flow. Their bottom (upstream) part remains spherical while their top (downstream) part narrows down and elongates along the direction of motion, resulting in pear-like shapes or in the reversible formation of a micron-size tube at the vesicle top. The sedimentation velocity of vesicle is very similar to that of a rigid sphere. Using a thermodynamic approach, we show that the hydrodynamic force acting at the top of a floppy vesicle can exceed the critical force needed to draw a membrane tube. We predict that the tube radius scales as the power 1/3 of the ratio of the bending energy to the typical hydrodynamic stress, $\eta U/R$ where η is the fluid viscosity, U is the sedimentation velocity and R the vesicle radius. This result is consistent with the reported experimental data. The tensions of vesicles exhibiting a tube and of pear-like shape are deduced from the thermodynamic approach.

1. Introduction

The behavior of living cells submitted to an external force or a hydrodynamic flow is an important issue both for physiology and for in-vitro processing and manipulation. It has been much studied for cells and giant lipid vesicles. The latter are basic soft shells whose behavior is a physical reference for the cell 'passive' behavior. For instance, in a shear or an elongational flow, giant vesicles and red blood cells present a variety of motions and deformations whose commonalities and differences have been characterized and understood on the basis of the specificity of the mechanical properties of each particle [1, 2, 3]. Another example is the behavior of vesicle and cell membranes subjected to an external pulling point force. It is well known that there is a critical force for which a nanotube, called tether [4,5,6,7,8,9] is drawn from the vesicle/cell and coexists with the spherical body of the particle. In-vivo, tether formation is involved in many biological processes such as intracellular trafficking [10,11,12] or cell migration [13]. In-vitro, tethers extruded from the membrane (by pulling a small bead adhering on the membrane) are used as sensors to gain information on vesicle/cell mechanical properties (cortical tension, coupling energy between the membrane and the cytoskeleton) [14,15,16,17].

Highly surprising, the behavior of vesicles and cells suspended in a fluid and submitted to a gravitational force is not thoroughly documented. One theoretical study [18] predicts that sedimenting vesicles should deform and present either pear-like shapes or bean-like shapes, with no experimental

* Author to whom any correspondence should be addressed

support. However, the question of the movement of deformable objects due to a body force in a viscous fluid, arises naturally in different situations such as centrifugation, magnetophoresis or cell sorting in microfluidics. For instance, recent observations of red blood cells during centrifugation show how the cells resume very peculiar pear-like shapes [19]. In a more general point on view, sedimentation and shape instability of simple viscous drops had also been observed. While a spherical drop remains spherical during sedimentation (the sphere is a steady solution to the Stokes equations [20]), non-initially spherical drops are unstable [21] and prolate shapes can develop long tails at their rear [22,23,24]. Initially spherical droplets can also be destabilized when surfactants are present. In this case, the flow gathers the surfactants at the rear of the droplet reducing drastically the local surface tension and leading to tip streaming [25].

In this paper, we study the deformation of giant unilamellar vesicles (GUVs) sedimenting in a quiescent fluid. We deal with very deformable floppy vesicles. We show that, depending on their sedimentation velocity, the vesicles present either original pear-like shapes, or, above a critical hydrodynamic force, develop at a micro-size lipid tube, which coexists with a quasi-spherical shape. A striking point is that the tube extraction does not require the application of a point force. The distributed hydrodynamic stress, which is much weaker than point forces generally used to extract tethers, is however sufficient to pull micron-size tubes on floppy vesicles. We show that a free energy analysis describes such a behavior.

We first detail the materials and method before describing the regimes of motion and the deformations of the vesicles. Then we show that vesicle velocities are similar to that of rigid spheres translating in a quiescent fluid. We propose an approach to describe and understand the formation of membrane tubes. Finally, we estimate and discuss the values of the surface tensions of sedimenting vesicles.

2. Experimental

2.1. Giant Unilamellar Vesicles (GUVs) preparation

GUVs are prepared by the electroformation method [26]. Dioleoyl-phosphatidylcholine (DOPC, Sigma) dissolved in chloroform and methanol solutions (9:1 volume ratio) at 2mg/ml and 10 μl of the solution is spread on the conductive faces of two transparent glass plates coated with a film of indium tin oxide (ITO). After drying (2h under primary vacuum), about 2ml of a sucrose solution (with concentration 300mM) is injected in a chamber formed by the ITO plates facing each other, separated by Teflon spacers and connected to an AC generator (frequency 10 Hz). The potential is very slowly increased from 0.2 to 0.8 V and kept constant for one night. The frequency and the voltage are finally decreased to 4 Hz and 0.2 V to detach vesicles from the ITO plates.

The suspension of vesicles we obtain is then diluted in a binary sucrose/glucose solution with the following protocol: 100 μl of the initial sucrose suspension of vesicles is diluted in 1 ml of the chosen binary sucrose/glucose solutions for 1 hour. Then, 100 μl of this suspension is rediluted in 1 ml of the binary sucrose/glucose solution for another hour. Finally 100 μl of this suspension is diluted again in 450 μl in the binary sucrose/glucose solution and is gently introduced in the observation chamber (volume 0.550 ml). Only few vesicles are present in the observation chamber in order to limit hydrodynamic interactions. The characteristics of the vesicles are listed in Table 1 and Table 2.

2.2. Method of observation

We use a parallelepiped chamber from Hellma (Mullheim, Germany) which has four optically transparent faces (width x-direction:10 mm, length y direction: 55 mm, height z-direction: 1 mm). Sedimenting vesicles and their reflections on the bottom of the chamber are observed in the vertical y-z plane, from a microscope (LEICA IRB) tipped to the horizontal [27]. We let the vesicles settle at the bottom of the chamber during 20 min. Then, we turn the chamber upside down and observe the sedimentation of one vesicle using a CCD camera (COHU 4910, 25 fps). In order to prevent vesicle adhesion on the chamber wall, we first incubated a casein solution in the chamber before introducing the vesicles. The vesicles were found to behave similarly in the chamber rinsed in Millipore water and in the chamber treated with casein. We therefore perform most experiments by simply using the chamber rinsed with Millipore water.

Movies are saved using a digital videocassette recorder SONY DSR25. Vesicle tracking, contour and

center of gravity determinations as well as shape analysis are carried out with the software IDL. The volume V and area A of the vesicles are measured at rest from the shapes of the settled vesicles. The effective radius R is deduced as $(3V/4\pi)^{1/3}$.

3. Observations

3.1. Full experiment

Typical experiments are shown in figure 1. First, the vesicle departs from the top of the chamber and progressively elongates and deforms while its velocity increases. Then a stationary regime is reached: the vesicle, located halfway the observation chamber, has a constant velocity and a stable shape. Finally, upon approaching the bottom wall, the vesicle velocity decreases and its shape progressively changes (no more vertical elongation). Then, upon landing on the bottom of the chamber, the vesicle flattens down with a typical gravity-induced shape deformation. When a tube is observed at the top of the vesicle, it retracts and it is swallowed by the main body of the vesicle during the landing stage, as shown by the last images of each sequence represented in Fig. 1.

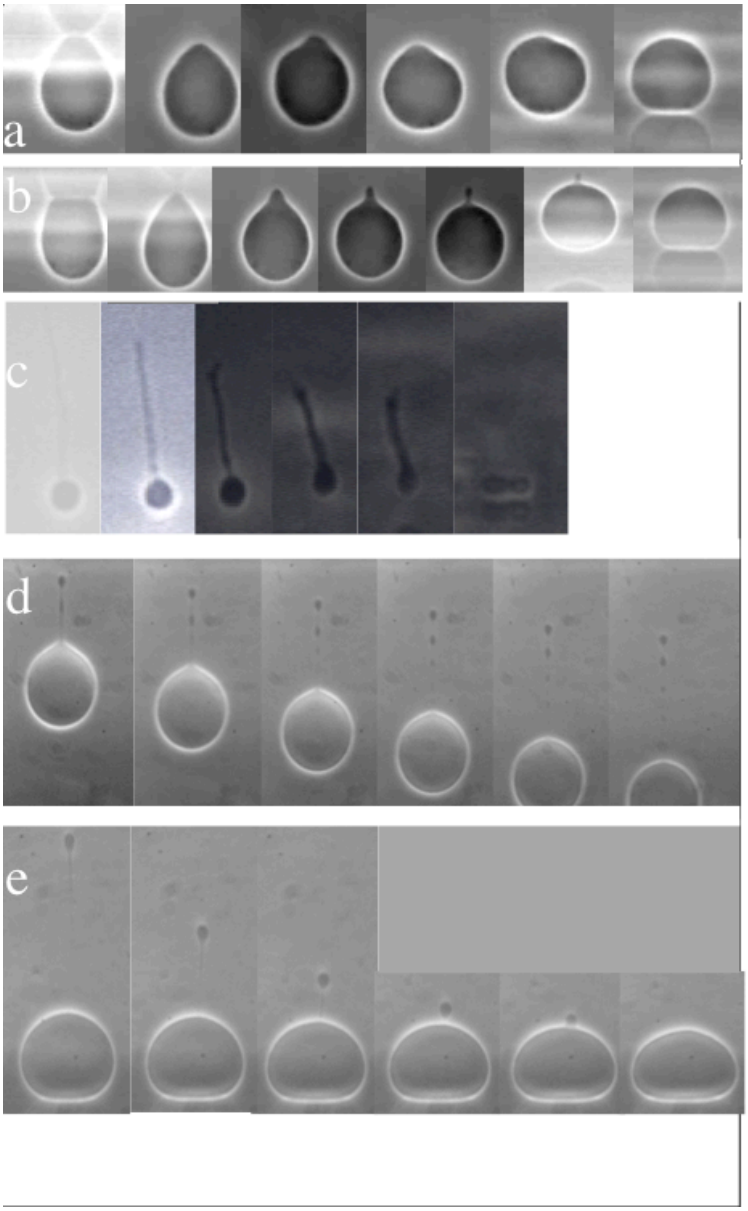

Figure 1: Vesicle sedimentation a: vesicle (2.2), pear shape, full process from departing to landing, t=

0s, 0:57 s, 2:22 s, 4:46 s, 5:08 s, 6:28 s, shapes are fluctuating. b: vesicle (12.1), short tube, full process, t=0s, 0:24s, 1:04s, 1:49s, 2:51s, 4:38s, 6:14s. c: vesicle radius 6 μm, landing process from stationary shape to settled vesicle, t=4:40s, 5:32s, 7:04 s, 8:30s, 9:12s, 12:00s. d: departing of a vesicle (radius 49 μm) and tube growth (time between image = 1s) e) landing of the vesicle with tube retraction (60s, 76 s, 84s, 90s, 92s, 93s).

3.2. Stationary shapes

Vesicles, which do not present large excess area cannot significantly deform and thus remain spherical during their sedimentation. However, most vesicles are osmotically deflated and are therefore floppy and deformable. We now describe their stationary shape. The vesicles exhibit a spherical upstream (bottom) region and a vertically elongated downstream (top) part with a radius of curvature, r, smaller than the spherical part. Weakly deformable vesicles present an egg-shape. More deformable vesicles look like pears with, at their top, a spherical cap of radius $r < R$ and an elongated region of length $L \leq r$ (figure 2). Some vesicles present a spherical part, which coexists with a tube. The tube radius, $r << R$, ranges from less than one micron to 2-3 microns. It is slightly pinched at its basis and, as seen in figure 1b and in figure 2, a catenoid shape is observed at the junction between the spherical part and the tube. Its length L is longer than r. Most of these vesicles present large membrane undulations (figure 1a), disclosing that the tension is very low. Some vesicles, which are characterized by the highest sedimentation velocities, exhibit several tens of microns long pearling tubes of submicron radius (figure 1d).

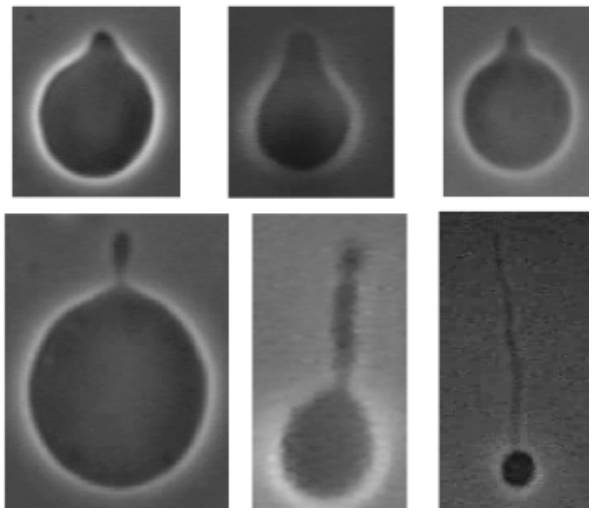

Figure 2 Typical stationary vesicle shapes. Top, pear-like shapes: (1.2) Radius 26 μm, (14.2) Radius 13 μm, (6.2) Radius 32 μm ; bottom, vesicles with tubes: (11.1) Radius 30 μm, (13.1) Radius 16 μm ; Radius 16 μm .

When vesicles are submitted to two or three successive experiments of sedimentation, similar shape deformations and sedimenting velocities are retrieved.

Finally it is worth noting that there is no lipid flow on the membrane surface as attested by small lipid aggregates bound to the membrane, which do not move relatively to the center of mass of the vesicle. Indeed, the driving force of the motion being vertical, the vesicles present a vertical axis of symmetry. This symmetry prevents the apparition of a lipid recirculation on its surface. Moreover, contrarily to a fluid drop, the two-dimensional confinement of lipid molecules and the symmetry of the experiment prevent any momentum transfer to the inner fluid and therefore no flow recirculation is observed.

4. Velocities

We show in this section that the velocity field around a sedimenting vesicle is given by the flow produced around a rigid sphere with a radius equal to the effective radius of the vesicle and shows that

at the leading order, the deformation of the vesicle does not modify the velocity field of the equivalent sphere.

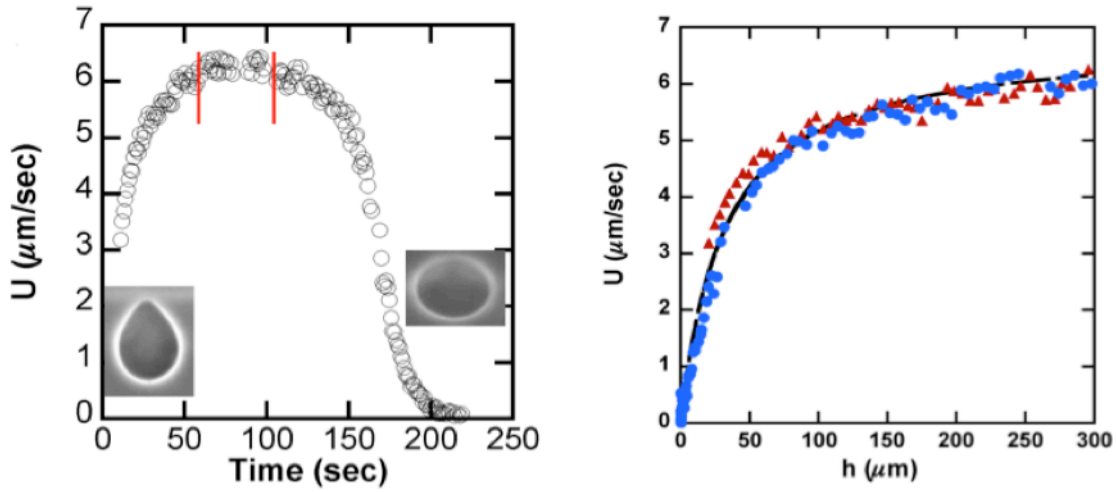

Figure 3 a : velocity versus time, the steady regime is reached in the middle of the chamber, b : velocity during (▲) departing of the vesicle from the top substrate, (●) landing of the vesicle to the bottom substrate and (—) equation 1; h is the distance between the vesicle membrane and the top wall (during departing) or between the vesicle membrane and the bottom wall (during landing).

The evolution of the vertical velocity of the center of mass of the vesicles as a function of time is illustrated in figure 3a for one pear-like shape vesicle. The existence of the stationary regime is clearly observed (Fig. 3a). The two transient regimes correspond to the departing and to the landing of the vesicle and the associated velocities are represented in figure 3b as a function of the distance h to the departing or the landing wall of the chamber. In comparison, we also plot the sedimentation velocity U of the equivalent sphere given by the following law:

$$U = \frac{2g}{9}\frac{\Delta\rho R^2}{\eta\left(1+\frac{R}{h}\right)}, \qquad (1)$$

where Δρ is the difference of density between the inner fluid of the sphere and the outer suspending fluid and g is the gravitational acceleration. U is derived from the approximated expression of the drag force of a rigid sphere moving close to a wall perpendicular to the direction of the sphere motion [28]. One can clearly see that departing and landing velocities are pretty similar and are well described by (1). This result shows that the deviation of the vesicle shape from a sphere does not affect the velocity field around the particle.

To confirm this result, we also plot the stationary velocity U observed far from the walls for all studied vesicles, whatever their shapes and for an spherical bead of agarose (R= 36 μm) as a function of $\frac{g}{9}\frac{\Delta\rho R^2}{\eta}$. All data lie on a single line as shown in figure 4. This result confirms that the vesicle behave like rigid spheres in a Stokes flow while its surface is an incompressible two-dimensional fluid. Because the lipids cannot leave the interface, the divergence of the velocity field is exactly zero. This strong constrain does not exist for a liquid drop where the molecules can leave the interface and transfer momentum to the volume even in an axisymmetric case. A liquid drop has therefore a lower

friction force than the fluid vesicle.

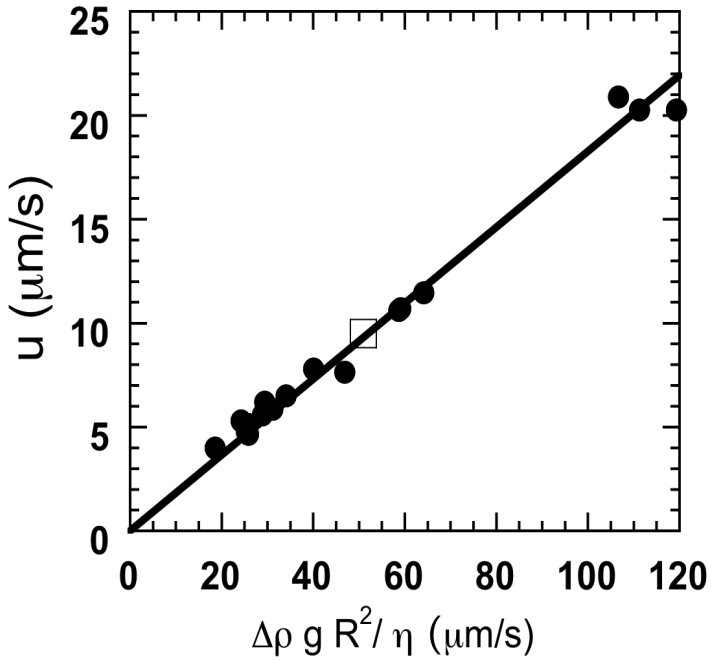

Figure 4. Variation of the translation velocity observed for different vesicles in the steady state versus $\Delta\rho\ g\ R^2/\eta$, square: velocity of an agarose rigid bead (R= 36 μm, Δρ=1.0466).

As a consequence, we will consider in a first approximation, that the drag force that applies on a sedimenting vesicle far from the walls is equal to the Stokes drag acting on a rigid sphere of equivalent radius: $6\ \pi\ \eta\ R\ U$.

5. Shape deformation: detailed description

The sedimentation of a vesicle generates an excess pressure upstream and a lower pressure downstream, at its top. This difference of pressure is at the origin of the pear-shape deformation. The viscous forces exerted by the fluid on the vesicle membrane redistribute a part of the membrane excess area toward the top part of the vesicle and under some conditions are able to draw a membrane tube. Using the pressure field around a rigid translating sphere [29], we can express the variation of the pressure p on the surface of the vesicle at a distance R from the center of mass:

$$p = p_\infty - \frac{3}{2}\eta \frac{\vec{U}.\vec{n}}{R}, \qquad (2)$$

where p_∞ is the pressure in the fluid far from the vesicle and $\vec{n}$ is the normal to the membrane. The difference of pressure between the top and the bottom part of the vesicle is therefore $3\ \eta\ U/R$, which is typically of the order of 10^{-3} Pa in our study.

5.1 Hydrodynamic tube extrusion

We consider the tube observed on the top of the vesicles in the stationary regime, i. e. when r <<R and L > r. We write the free energy of the tube membrane by using the approach developed by Waugh et al. [7,30,31], Evans et al. [32], Derényi et al. [33], Hochmuth et al. [16], Brochard-Wyart et al. [8] and Fournier [34]. It is based on the Helfrich Hamiltonian, which describes the membrane as a fluid, incompressible surface with a homogeneous surface tension σ and a bending rigidity κ. For a fixed tension and a fixed pressure, the tube free energy F of radius r and length L can be written as

$$F = \left(\frac{\kappa}{2r^2} + \sigma \right) 2\pi\, r\, L - \Delta p\, \pi\, r^2\, L - f\, L, \tag{3}$$

where Δp is the pressure difference across the tube membrane and f is the pulling force, which elongates the tube on a length L.
We consider that the thickness of the membrane is constant. Then, the area difference between the lipid inner monolayer and the outer monolayer of the membrane changes when a tether is pulled out. The change in area difference creates a spontaneous curvature of the membrane calculated in reference [35]. The energetic cost for this curvature was estimated in [36] to $\approx \kappa\, L^2 / R^2$, where R is the vesicle radius. This contribution is significant only for tube lengths of more than 100 microns so that we omit it in the free energy.
The tube radius and the pulling force are calculated at equilibrium by taking $\frac{\partial F}{\partial r} = 0$ and $\frac{\partial F}{\partial L} = 0$.
The first derivative gives the equilibrium Laplace law for a cylinder:

$$\frac{\sigma}{r} - \frac{\kappa}{2r^3} = \Delta p \tag{4}$$

We estimate the pressure difference across the tube membrane by considering that the hydrostatic pressure out of the tube is roughly equal to the pressure upstream at the vesicle top: $\Delta p = p_{in} - (p_\infty - 3\, \eta\, U/2R)$, where p_{in} is the pressure within the vesicle. Here, the vesicles are initially tensionless since they have been deflated. In this case, the difference of pressure $p_{in} - p_\infty \approx 0 << 3\, \eta\, U/2R$. Therefore, (4) rewrites as

$$\frac{\sigma}{r} - \frac{\kappa}{2r^3} = \frac{3\eta U}{2R} \tag{5}$$

The surface tension of the vesicle is induced by the flow and is therefore of the order of the 'hydrodynamic' tension $\sigma \approx \eta U \approx 10^{-8}$ N/m. The pressure term in the right-hand term of (5) is one order of magnitude smaller ($\approx 10^{-3}$), than the tension and the bending term ($\approx 10^{-2}$) since tubes radii are much smaller ($r \approx 1$ μm) than R. The right-hand term of pressure of (5) plays therefore only the role of a small corrective factor.
If the vesicle is initially tense ($\sigma >> \eta U$), the pressure terms in (5) are not dominant. One retrieves the classical frame [8,33,34] $r = (\kappa/2\sigma)^{1/2}$, which yields a typical size for r of the order of 40 – 50 nm for a standard value of $\sigma \approx 10^{-5}$ N/m.
The second derivative $\frac{\partial F}{\partial L} = 0$ gives the classical value of the equilibrium pulling force exerted on the tube of radius r:

$$f_c = \frac{3\pi\kappa}{2r} + \pi\, r\, \sigma \tag{6}$$

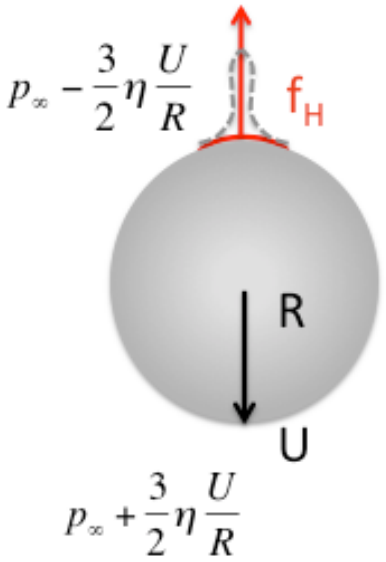

Figure 5 Schematic of a sedimenting vesicle.

The combination of the two equations (5) and (6) sets the equilibrium radius r_0 of the tube coexisting with a quasispherical vesicle and the associated equilibrium pulling force f_0.
In the case of a sedimenting vesicle, the force exerted on the vesicle surface is the drag force induced by the flow.
The pulling force, which initiates the tube is exerted on the top of a spherical cap of area S:

$$\vec{f}_H = -\frac{3\eta\vec{U}}{2R} S . \tag{7}$$

When this hydrodynamic force is equal to the extrusion force f_0 it is possible to draw a tube. The condition $f_H = f_0$ is

$$\frac{3\eta U}{2R} S = \frac{3\pi\kappa}{2r_0} + \pi r_0 \sigma \tag{8}$$

Noteworthy, equation 8 compares the critical force of extraction at a tension and for hydrodynamic conditions that are not exactly the one of the stationary regime. However, since we see a tube emerging for a value of the velocity close to 90% of the stationary regime, we believe that our approximation is valid.
We assume that the radius of this spherical cap is of the order of magnitude of the tube radius plus the crossover region that relates the quasi-spherical vesicle to the tube (red line in figure 5). As pointed out in [37] the crossover region is an exponentially damped sinusoid with a decay length of the order of r_0. We therefore write $S \approx \pi (\alpha r_0)^2$ with α being the only adjustable parameter, close to 2. By using (5) and (8) to eliminate σ, one obtains a relation for the equilibrium tube radius

$$r^3\left(\alpha^2 - 1\right) = \frac{4\kappa R}{3\eta U} \tag{9}$$

Figure 6 shows a plot of the parameter r^3 as a function of $\frac{4R}{3\eta U}$ measured for 13 vesicles of different sizes R (from 16 to 48.5 μm) and velocity U ranging from 4 to 12.5 μm/s. Data are fitted with (9) with

the slope, $\kappa/(\alpha^2 - 1)$, equal to 8.11 10^{-21} J. By setting that the bending rigidity $\kappa \approx 10$ kT = 4 10^{-20} J, which is a value currently accepted for DOPC membranes, we find that $\alpha = 2.45$, which is in good agreement with the prediction of the crossover region given in [37]..

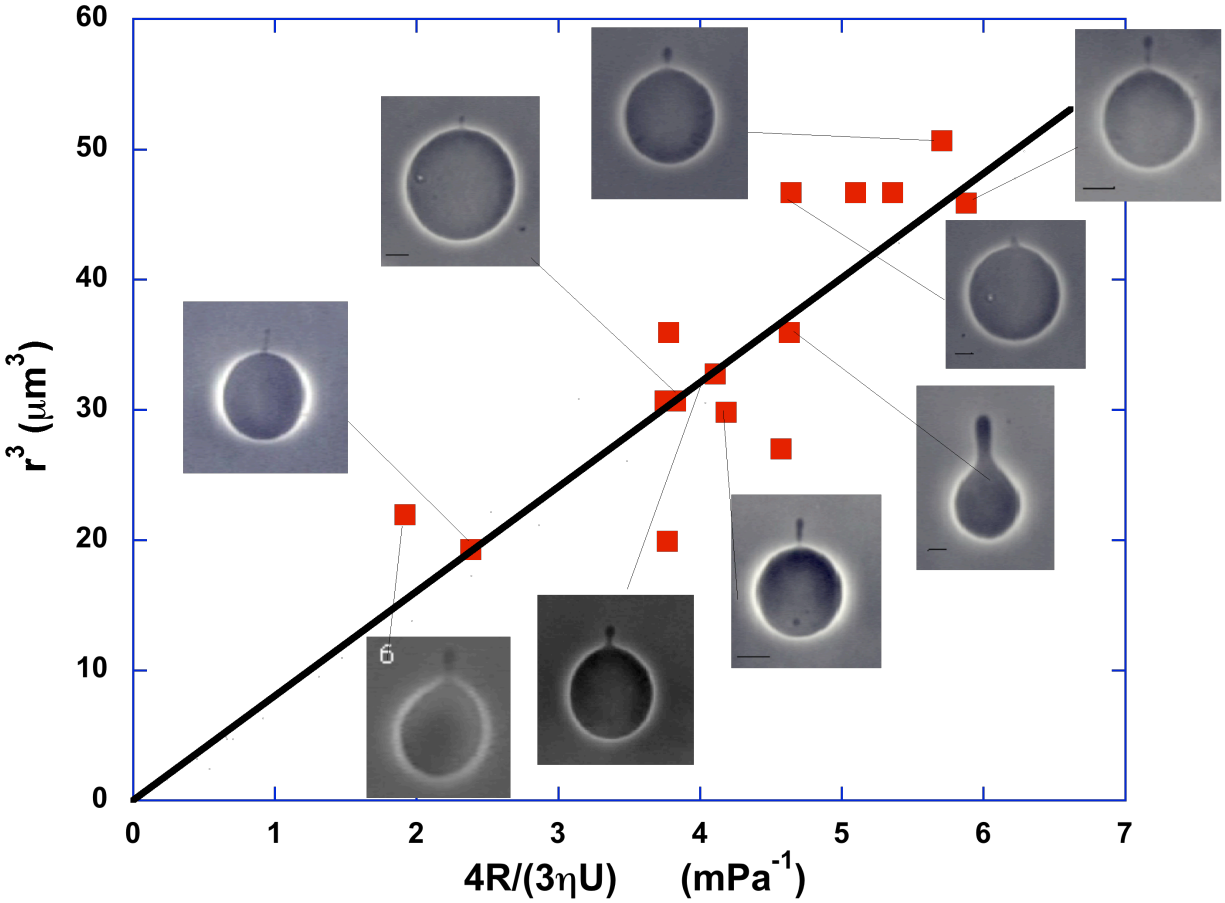

Figure 6: Variation of a parameter scaling as the cube of the tube radius versus the reduced variable 4R/3ηU. The straight line is the theoretical prediction from (9) with a slope equal to 8.11 10^{-21} J.

From the experimental measurements of the equilibrium tube radius and of the sedimenting velocity, we have estimated the tension of the 13 vesicles during their sedimentation from equations (5) and (8). They are very low (Table 2) as expected for floppy vesicles. Noteworthy, the force f_0 required to draw a tube from a floppy vesicle is quite small, of the order of 10^{-13} N.

For tensed vesicles, where the pressure term in equation (4) is neglectible, the same power law is retrieved, $r = \left(\frac{\kappa R}{6\eta U}\right)^{\frac{1}{3}}$ and the tension scales as $\sigma = \frac{\kappa^{\frac{1}{3}}}{2}\left(\frac{6\eta U}{R}\right)^{\frac{2}{3}}$. The velocity required to draw a tube from a vesicle of tension σ and bending energy κ is $U = \frac{R(2\sigma)^{\frac{3}{2}}}{6\eta\,\kappa^{\frac{1}{2}}}$.

In figure 7 we show the theoretical curves of variation of the ratio of the tube radius to the vesicle radius and of the adimensioned tension, $\sigma R^2/\kappa$ as a function of the adimensioned capillary number $\eta U R^2/\kappa$ for a vesicle drawing a tube.

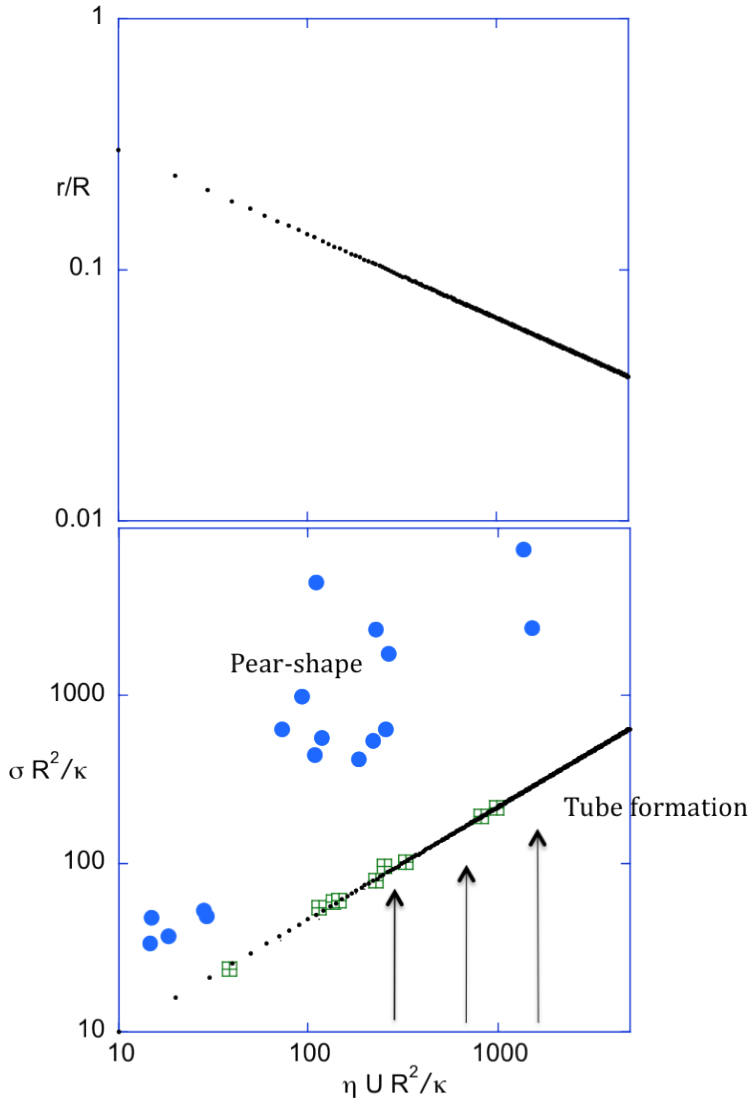

Figure 7 Theoretical curves (small dots) of variation of the ratio of the tube radius to the vesicle radius and of the adimensioned tension, $\sigma R^2/\kappa$ as a function of the adimensioned capillary number $\eta U R^2/\kappa$ for a vesicle drawing a tube. Filled circles correspond to pearlike vesicles (Table 2) where the tension is calculated from equation 12. Squares correspond to vesicles drawing a tube (Table 1), where the tension is calculated from equation 5. The bending energy is set equal to $4\ 10^{-20}$ J

In order to get an idea of the evolution of the vesicle tension during sedimentation, we measure its apparent surface area. When the tension increases, the apparent vesicle area A also increases unfolding the submicron thermal fluctuations of the membrane. We plotted in figure 8 the parameter $R_{Area} = (A/4\pi)^{1/2}$ as a function of time. While decelerating just before landing the vesicle reduces its area, which reaches a minimum, revealing a minimal surface tension. At this stage, the vesicle flattens and swallows the tube. Then, the area increases again when the vesicle settles onto the substrate and reaches a value similar to that observed during the steady sedimentation stage. Vesicle tensions falling steadily in a fluid or settled onto a substrate are similar. This is not a surprise since the vesicle is submitted in both cases to the same gravitational force. In one case the reaction is the drag force while in the other case it is the reaction of the substrate. The vesicle area and volume are similar in both cases but the repartition of the force is different, yielding different shapes.

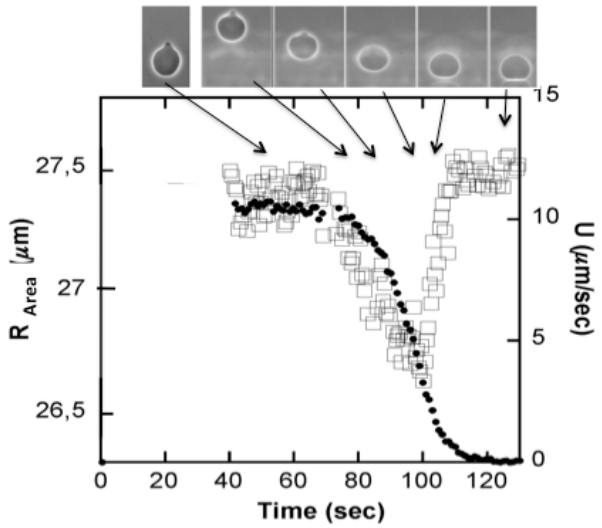

Figure 8: Variation of $(A/4\pi)^{1/2}$ (□) and the velocity (●) versus time. Top: pictures of the vesicle at various times of the sedimentation process.

The tube comes from the change of the repartition of the volume and the surface area of the vesicle with respect to the shape of the vesicle settled at the bottom of the chamber. It is possible since the vesicle presents an excess of area. It is characterized by the reduced volume,

$$v = \frac{3V}{4\pi\left(\frac{A}{4\pi}\right)^{\frac{3}{2}}}$$

defined as the ratio of the volume of the vesicle relatively to the volume of the sphere with the same surface area ($v \leq 1$, $v = 1$ for a sphere), where V is the vesicle volume. It is deduced from azimuthal integration over the contour of the vesicle settled on the substrate by applying the Papus-Guldin theorem (assuming an axisymmetric shape) [38]. The length of the tube L can be then estimated by expressing the overall volume spherical part + the tube part as $V= 4\pi R^3/3 + \pi r^2 L$, and the surface area as $A=4 \pi R^2 + 2\pi rL$ and by replacing V and A in the expression of the reduced volume. This yields

$$v = \left(R^3 + \frac{3}{4}r^2 L\right)\left(1+\frac{rL}{2R^2}\right)^{-\frac{3}{2}} R^{-3} \qquad (10)$$

After linearization, we obtain the expression of the tube length,

$$L = \frac{4}{3}\frac{R^3(1-v)}{r(vR-r)} \qquad (11)$$

Figure 9 shows the plot of L measured as a function of the reduced parameter $\frac{4}{3}\frac{R^3(1-v)}{r(vR-r)}$ for the 13 vesicles, which exhibit micron-size tubes. The agreement with the theoretical curve, without any adjustable parameter is quite good.

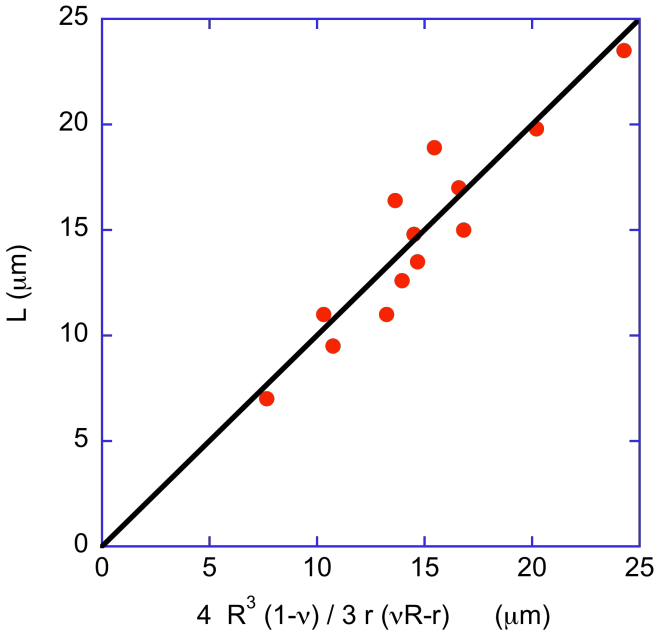

Figure 9 Experimental tube length versus a reduced parameter (see text). The straight line of slope 1 is the theoretical prediction.

5.2. Egg and Pear-like shape vesicles

When the sedimenting velocity of a vesicle is too small, the hydrodynamic force is smaller that the critical force required to extrude a tube. This happens for the couples (σ, ηU) located above the curves displayed in figure 7. The vesicle deforms but no tube is extruded at its rear. Because the external pressures at the bottom and at the top part of the vesicle are different, the curvature radii at the top and at the bottom of the vesicles are different, generating egg or pear-like shapes.

We propose to calculate the tension of little extended objects like egg and pear-like vesicles. With a good approximation we can describe the bottom and the top of the vesicle by two spherical caps of radius R and r_{top} respectively. In this case, we can roughly estimate the vesicle surface tension by writing the Laplace law on both spherical parts:

$p_{in} - p_\infty - 3\,\eta\,U/2R = 2\,\sigma_{bot}/R$ and $p_{in} - p_\infty + 3\,\eta\,U/2R = 2\,\sigma_{top}/r_{top}$. The flow imposes a pressure gradient inside the membrane surface, which compensates the applied viscous force per unit area. The tension difference between bottom and top endcaps is equal to $3\eta U$: $\sigma_{bot} - \sigma_{top} = 3\eta U$, leading to the following relation between the velocity, the radii and the tension:

$$\sigma_{top} = \frac{9\eta U\, r_{top}}{2\left(R - r_{top}\right)} \qquad (12)$$

We measured values of R and r_{top} on 18 egg and pear-like vesicles and we estimated the membrane surface tension of the vesicles, which are reported in Table 2..

In figure 7b, we plot the reduced tension of these vesicles as a function of the capillary number $\eta\, U\, R^2/\kappa$ to obtain a phase diagram. The domain of coexistence at equilibrium of a tube and a spherical vesicle is on the black curve. The pear like regime lies in the highest part of the diagram, above the curve of coexistence tube-vesicle. Below the coexistence curve, the vesicles are initially floppy and are not in equilibrium: a tube is initiated, which grows and increases the vesicle tension. The length of the tube stops when the tension reaches the equilibrium coexistence tension. In our case, most vesicles exhibit large excess area but are slightly tensed due to the gravity.

Conclusion

We have shown that the drag force is able to draw a tube from the top of a vesicle sedimenting in a quiescent fluid while it is not a point force as usually described in the literature for membrane tethers extrusion. In our study we used vesicles, which were osmotically deflated before the experiments, and were characterized by very small (vanishing) surface tensions. In this case the critical force to extrude a tube is very small, of the order of 10^{-13}N, and a vesicle moving at a few μm/s can develop tubes with micron-size radii. Noteworthy, no force barrier seems to exist for the formation of tubes, contrarily to the case of tube formation by application of a point force, where the force barrier grows linearly with the size of the area the force is exerted on 39.
With a classic thermodynamic approach, we proposed a basic model, which predicts that the tube radius varies as $r = \left(\frac{\kappa R}{6\eta U} \right)^{\frac{1}{3}}$ consistently with reported experimental data. For large tensions, we predict that the velocity required to draw a tube increases with the power 1.5 of the surface tension.

These results may be of importance when GUVs are subjected to centrifugation, as it is the case in the recent method called double emulsion used to prepare vesicles. In this case, the vesicle velocity can reach several hundreds of μm/s and can generate the formation of membrane tubes.
Finally we hope that our work will stimulate numerical more detailed theoretical descriptions able to predict all the observed shapes of vesicles, from the existence of tubes to pearlike shapes, within a single frame.

Acknowledgments: We want to thank J. B. Fournier and J. M. Allain for stimulating discussions. The labs belong to the CNRS consortium CellTiss.

Table 1 Characteristics of vesicles with a tube

#	Vesicle radius R (μm)	Tube radius r (μm)	Length tube (μm)	Velocity U (μm.s^{-1})	Viscosity η (10^3 Pa.s)	Density Δρ (g.l^{-1})	Reduced volume ν	Calculated tension from eq. 5 σ (10^8 N.m^{-1})
1.1	30.5	2.71	7	8.11	1.33	7.4	0.985	0.42
2.1	25	3	11	5.48	1.33	7.4	0.96	0.35
3.1	25.8	3.1	16.4	6.18	1.33	7.4	0.96	0.36
4.1	29.5	3.6	18.9	4.93	1.36	4.4		0.28
5.1	48.1	3.1	9	12.4	1.36	4.4	0.99	0.37
6.1	48.5	3.3	11	10.2	1.37	3.2	0.99	0.33
7.1	34	3.7	14.8	5.97	1.33	4.2	0.97	0.28
8.1	28.6	2.7	12.6	12.4	1.29	11	0.97	0.5
9.1	17.5	3.6	23.5	4	1.26	10		0.31
10.1	30.3	3.6	17	5.87	1.33	4.2	0.959	0.29
11.1	28.5	3.2	19.8	7.64	1.29	6.7	0.95	0.35
12.1	25.3	3.6	13.5	5.3	1.36	4.4	0.95	0.3
13.1	16	2.8	15	9.5	1.17	18	0.9	0.5

Table 2 Characteristics of pear or egg like vesicles

#	Bottom radius R (μm)	Top radius r (μm)	Velocity U (μm.s^{-1})	Viscosity η (10^3 Pa.s)	Density Δρ (g.l^{-1})	Calculated tension from eq. 12 σ (10^8 N.m^{-1})
4-1.2	25.4	8.5	10.63	1.29	11	3
5-2.2	26.4	12.6	4.66	1.33	4.2	2.7
6-3.2	27.2	14	4.8	1.33	4.2	3
7-4.2	44.8	24.4	20.9	1.3	7	13.2
8-5.2	23.5	15.5	4	1.31	4	4.5
2-6.2	30	8.9	6.2	1.33	4.2	1.5
10-7.2	24.3	22	5.6	1.33	7.4	33
11-8.2	48	13	20.27	1.29	11	4.5
13-9.2	25.7	18.2	10.7	1.29	11	15
14-10.2	21	14.75	6.5	1.29	11	9
18-11.2	10.7	2.2	2.9	1.17	18	0.3
19-12.2	12.8	4	3.8	1.17	18	0.9
20-13.2	13.7	3.8	6	1.17	18	1.2
21-14.2	12.9	3.3	7.1	1.17	18	1.2
23-15.2	23.8	8	15.6	1.17	18	4.2
0522 V17 16.2	15	5	3.2	1.26	10	1.3
0521 10 17.2	32.2	19.2	7.91	1.30	7	6.9
070520 5 18.2	15	4	3	1.33	7.4	0.9

1 Abkarian M and Viallat A 2008 *Soft Matter* 4 653
2 Pozrikidis 2003 *Modeling and Simulation of Capsules and biological Cells* (Chapman & Hall/CRC Mathematical Biology and Medecine Series)
3 Deschamps J , Kantsler V , Segre E and Steinberg V 2009 *PNAS* 106, 28 11444
4 Waug R 1982 *Biophys. J.* 38 29
5 Hochmuth R M, Mohandas N and Blackshear P L 1973 *Biophys. J.* 13 747
6 Hochmuth RM, Wiles H C, Evans E A and McTown J T 1982 *Biophys. J.* 39 83
7 Bo L and Waugh R 1989 *Biophys. J.* 55 509
8 Brochard-Wyart F, Borghi N and Nassoy P 2006 *PNAS* 103 7660
9 Kremer S, Campillo C, Pepin-Donat B, Viallat A and Brochard-Wyart F 2008 *Europhys. Lett.* 82 48002
10 White J, Johannes J, Mallard F, Girod A, Grill S, Reinsch S, Keller P, Tzschaschel, Echard A and Goud B 1999 *J. Cell Biol.* 147 743
11 Cooper M, Cornell-Bell A, Chernjavsky A, Dani J and Smith S 1990 *Cell* 60 135
12 Rustm A, Saffrich R, Markovic I, Walther P and Gerdes H H 2004 *Science* 303 1007
13 Schmidtke D W and Diamond S L 2000 *J. Cell. Biol.* 149 719
14 Waugh R and Bauserman R 1995 *Ann. Biomed. Eng*. 23 308
15 Shao J-Y and Hochmuth R M 1996 *Biophys. J.* 71 2892
16 Hochmutn R M , Shao J-Y, Dai J and Sheetz M P 1996 *Biophys J.* 70 358
17 Li Z, Anvari B, Takashima M, Brecht P, Torres J H and Brownell W E 2002 *Biophys. J.* 82 1386
18 Kern N and Fourcade B 1999 *Europhys. Lett.,* 46 (2) 262
19 Hoffman J F and Inoué S 2006 P*NAS* 103 2971
20 Batchelor G. K. 1967. *An Introduction to Fluid Dynamics.* Cambridge: Cambridge Univ. Press.
21 Kojima M, Hinch E J and Acrivos A 1984 *Phys. Fluids* 27 19
22 Koh C J and Leal L G 1989 *Phys. Fluids* A1 8 1309
23 Koh C J and Leal L G 1990 *Phys. Fluids* A2 12 2103
24 Pozrikidis, C. 1990. *J. Fluid Mech.* 210 1
25 Johnson R A and A Bohran 2000 *Phys. Fluids* 12, 773
26 Abkarian M, Lartigue C and Viallat A 2001 *Phys. Rev. E*., 63, 041906
27 Abkarian M and A. Viallat, 2005 *Biophys. J.* 89 1055
28 Guyon E, Hulin J P and Petit L 2001 *Hydrodynamique Physique,* edp science
29 Landau L D and Lifshitz E M 1987 *Fluid Mechanics* vol 6 (1rst ed.), Butterworth-Heinemann, ISBN 978-0-080-33933-7.
30 Waugh R and Hochmuth R 1987 *Biophys. J.* 52 391
31 Waugh R, Song J, Svetina S and Zeks B 1992 *Biophys. J.* 61 974
32 Evans E and Yeung A 1994 *Chem Phys Liquids* 73 39
33 Derényi I, Jülicher F and Prost J 2002 *Phys. Rev. Lett.* 88 238101
34 Fournier J B 2007 *Soft Matter* 3 883
35 Bozic B, Svetina S, Zeks B and Waugh R 1992, *Biophys. J.* 61 963
36 Borgi N 2006 *PhD Thesis* Université Paris 6, France
37 Powers T R, Huber G and Goldstein R E, 2002 *Phys. Rev. E,* 65 041901
38 Abkarian M and Viallat A 2005 *Biophys. J.* ; Kern W. F. and Bland. J. R. 1948 *Theorem of Pappus. In Solid Mensuration with Proofs*, 2nd Ed. Wiley, New York, NY. p 110
39 Koster G, Cacciuto A, Derenyi I, Frenkel D and Dogterom M 2005 *Phys. Rev. Lett.,* 94 068101